Journal of The Electrochemical Society, **158** (5) A611-A618 (2011)
0013-4651/2011/158(5)/A611/8/$28.00 © The Electrochemical Society

Modeling the Dependence of the Discharge Behavior of a Lithium-Ion Battery on the Environmental Temperature

Ui Seong Kim,[a] Jaeshin Yi,[a] Chee Burm Shin,[a,*,z] Taeyoung Han,[b] and Seongyong Park[c]

[a]*Department of Chemical Engineering and Division of Energy Systems Research, Ajou University, Suwon 443-749, Republic of Korea*
[b]*Vehicle Development Research Laboratory, GM R&D Center, Michigan 48090-9055, USA*
[c]*Advanced Technology Team, GM Daewoo Auto & Technology, Inchon 403-714, Republic of Korea*

This paper reports a method of modeling the dependence of the discharge behavior of a lithium-ion battery (LIB) on the environmental temperature. A comparison of the experimental discharge curves for discharge rates ranging from 0.5 to 5 C and environmental temperatures of 15, 25, 35, and 45°C with the modeling results validates the two-dimensional modeling of the potential and current density distributions on the electrodes of an LIB as a function of the discharge time during galvanostatic discharge based on the finite element method. The heat generation rates as a function of the discharge time and the position on the electrodes are calculated to predict the temperature distributions of the LIB based on the modeling results of the potential and current density distributions. The temperature distributions obtained from the modeling are in good agreement with the experimental measurements.
 [DOI: 10.1149/1.3565179]

Manuscript submitted November 12, 2010; revised manuscript received February 19, 2011. Published March 28, 2011.

The lithium-ion battery (LIB) is a preferred power source for hybrid electric vehicles (HEVs) and electric vehicles (EVs) due to its high energy density, high voltage, and low self-discharge rate. The battery management system (BMS) plays a vital role in HEV and EV applications, since the accuracy of battery management algorithms has a significant impact on the performance and life of batteries. The BMS of HEV and EV propulsion systems needs to be based on an accurate model to predict the performance of the battery as a function of its temperature, as the battery performance depends strongly on its temperature. Therefore, it is crucial to develop a reliable model to predict the temperature dependence of the performance of LIBs in order to optimize battery management algorithms.[1–3]

There have been many previous works on the modeling of lithium-based batteries.[4–21] Doyle et al.[4] developed a model of the galvanostatic charge and discharge of the lithium polymer battery (LPB) using the concentrated solution theory. Doyle and Newman[5] presented a simplified model of an ohmically-dominated porous electrode with no diffusion or kinetic limitations to describe the discharge of an LPB. Chen and Evans[6–8] developed two and three dimensional models to study the thermal behavior of LPBs and LIBs. They assumed that the heat generation rate is uniform throughout the cell. Pals and Newman presented a one-dimensional model to predict the thermal behavior of LPBs for a single cell[9] and a cell stack.[10] Verbrugge[11] modeled the three-dimensional current and temperature distributions in LPB modules. Botte et al.[12] used a mathematical model that includes the carbon anode decomposition reaction to predict the thermal behavior of LIBs under medium- and high-rate discharge conditions. Al-Hallaj et al.[13] presented a simplified one-dimensional thermal modeling with lumped parameters to simulate the temperature profiles inside LIB cells. Song and Evans[14] developed an electrochemical-thermal model of LPBs by coupling a two-dimensional thermal model with a one-dimensional electrochemical model. Gu and Wang[15] and Srinivasan and Wang[16] developed a two-dimensional thermal and electrochemical coupled model to analyze the electrochemical and thermal behaviors of LIB cells. Gomadam et al.[17] reduced a two-dimensional heat conduction model to a one-dimensional model for LIB with a spiral geometry by a coordinate transformation approach. Chen et al.[18] developed a three-dimensional model of LIBs considering the location-dependent convection and radiation at the boundaries to reflect the different heat dissipation performances on all of the surfaces. Kim et al.[19,20] presented a two-dimensional thermal modeling based on the potential and current density distributions obtained by the same procedure as that described by Kwon et al.[21] Kim et al.[19,20] and Kwon et al.,[21] however, reported only the modeling results at the environmental temperature of 25°C and the validation of modeling through the comparison of modeling results with the experimental measurement data at 25°C. It is especially important to predict how the battery performance changes with the environmental temperature to design optimally the BMS in HEV and EV applications, because the variation range of environmental temperature is extensive depending on the circumstances in which the HEVs and EVs are operated.

In this work, a method of modeling the dependence of the discharge behavior of a LIB on the environmental temperature is presented. To accommodate the temperature dependence of the discharge behavior of a LIB, the key parameters obtained at the environmental temperature of 25°C in the modeling reported by Kim et al.[19,20] and Kwon et al.[21] are modified based on the well-known principles of the Arrhenius equation of chemical kinetics and the Nernst equation of electrochemical thermodynamics.[22] The modeling of the potential and current density distributions on the electrodes during discharge is validated by comparing the experimental and modeling discharge curves at various discharge rates ranging from 0.5 to 5 C under the environmental temperatures of 15, 25, 35, and 45°C. Then, the thermal behavior is modeled based on the potential and current density distributions on the electrodes as a function of the discharge current ranging from 0.5 to 5 C and the environmental temperature of 15, 25, 35, and 45°C. The thermal model is validated by comparing the temperature distributions of the battery cell obtained from the modeling with those of the experimental IR images.

Mathematical Model

A 14.6 Ah LIB comprising a $LiMn_2O_4$ cathode, a graphite anode, and a plasticized electrolyte from LG Chem. was modeled in this work. A cell consisting of two parallel plate electrodes of the battery shown in Fig. 1 was chosen because it consists of the same repeating units of positive and negative electrode plates, polymer electrolytes and separators. In Fig. 1, the current collecting tabs are the current collectors extending outside the rectangular electrodes and they do not contain the electrode (active) material. Figure 1 shows a schematic diagram of the current flow in the cell during charge. The distance between the electrodes was assumed to be so small that the

* Electrochemical Society Active Member.
z E-mail:cbshin@ajou.ac.kr

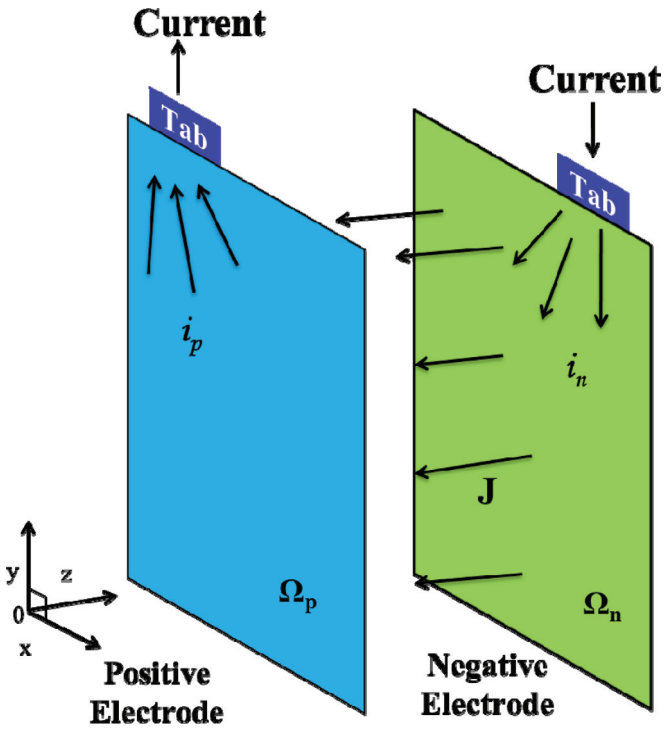

Figure 1. (Color online) Schematic diagram of the current flow in the parallel plate electrodes of a battery.

current flow between the electrodes is perpendicular to the electrodes. The modeling procedure used to calculate the potential and current density distribution on the electrodes was similar to that used by Kwon et al.[21] From the continuity of the current on the electrodes, the following equations can be derived

$$\nabla \cdot \vec{i}_p - J = 0 \quad \text{in } \Omega_p \qquad [1]$$

$$\nabla \cdot \vec{i}_n + J = 0 \quad \text{in } \Omega_n \qquad [2]$$

where $\vec{i}_p$ and $\vec{i}_n$ are the linear current density vectors [current per unit length (A m^{-1})] in the positive and negative electrodes, respectively, and J is the current density [current per unit area (A m^{-2})] transferred through the separator from the negative electrode to the positive electrode. Ω_p and Ω_n denote the domains of the positive and negative electrodes, respectively. By Ohm's law, $\vec{i}_p$ and $\vec{i}_n$ can be written as

$$\vec{i}_p = -\frac{1}{r_p}\nabla V_p \quad \text{in } \Omega_p \qquad [3]$$

$$\vec{i}_n = -\frac{1}{r_n}\nabla V_n \quad \text{in } \Omega_n \qquad [4]$$

where r_p and r_n are the resistances (Ω) of the positive and negative electrodes, respectively, and V_p and V_n are the potentials (V) of the positive and negative electrodes, respectively. The resistances, r_p and r_n, were calculated as described in Refs. 19–21. By substituting Eqs. 3 and 4 into Eqs. 1 and 2, respectively, the following Poisson equations for V_p and V_n are obtained

$$\nabla^2 V_p = -r_p J \quad \text{in } \Omega_p \qquad [5]$$

$$\nabla^2 V_n = +r_n J \quad \text{in } \Omega_n \qquad [6]$$

The relevant boundary conditions for V_p and V_n are given in Ref. 19.

The current density, J, of Eqs. 5 and 6 is a function of the potential difference between the positive and negative electrodes, $(V_p - V_n)$. The functional form depends on the polarization characteristics of the electrodes. In this work, the following polarization expression used by Tiedemann and Newman[23] and Newman and Tiedemann[24] was adopted

$$J = Y(V_p - V_n - U) \qquad [7]$$

where Y and U are the fitting parameters. As suggested by Gu[25], U and Y were expressed as functions of the depth of discharge (DOD) as follows

$$U = a_0 + a_1(DOD) + a_2(DOD)^2 + a_3(DOD)^3 \qquad [8]$$

$$Y = a_4 + a_5(DOD) + a_6(DOD)^2 + a_7(DOD)^3 + a_8(DOD)^4 + a_9(DOD)^5 \qquad [9]$$

where a_0–a_9 are the constants that provide the best fit of the modeling results to the experimental data at an environmental temperature of 25°C. The usual approach of linear or nonlinear parameter estimation cannot be used in this work, because the explicit functional relationship between the cell voltage and the values of a_0–a_9 is not identifiable. The approach adopted in this work is the "art" of trial and error, which may require exhaustive enumeration. One way to alleviate the efforts of trial and error is to use the low order polynomials of *DOD* in Eqs. 8 and 9 to obtain a rough fit of the experimental data and then to increase gradually the orders of polynomials to get a more refined fit. The values of a_0–a_9 used to calculate the potential and current density distribution on the electrodes are listed in Table I. In order to model the discharge behaviors at the different environmental temperatures other than 25°C, Y and U should be modified as follows

$$Y = Y_0 \exp\left\{-C_1\left(\frac{1}{T_{abs}} - \frac{1}{T_{abs,0}}\right)\right\} \qquad [10]$$

$$U = U_0 - C_2(T_{abs} - T_{abs,0}) \qquad [11]$$

where Y_0 and U_0 are the values of Y and U at an environmental temperature of 25°C, T_{abs} and $T_{abs,0}$ are the absolute temperatures (K) of the environment and 25°C, respectively, and C_1 and C_2 are constants to be determined to fit the temperature dependence of Y and U. The functional relationship of Y with T_{abs} suggested in Eq. 10 was deduced from the Arrhenius equation which gives the relationship between the reaction rate constant and the absolute temperature as shown below[22]

$$k = Ae^{-E_a/RT_{abs}} \qquad [12]$$

Table I. Fitting parameters used to calculate the potential and current density distributions on the electrodes.

Parameter	Value
a_0 (V)	4.12
a_1 (V)	−0.804
a_2 (V)	1.075
a_3 (V)	−1.177
a_4 (Am^{-2})	116.859
a_5 (Am^{-2})	−892.8001
a_6 (Am^{-2})	5250.46
a_7 (Am^{-2})	−13623.09
a_8 (Am^{-2})	15853.17
a_9 (Am^{-2})	−6757.8539

Table II. Parameters used for the thermal modeling.

Component	Density (g/cm^3)	Heat capacity (J/g·K)	Thermal conductivity (W/cm·K)	Ref.
Current collector of positive electrode	2.7	0.9	2.38	27
Electrode material of positive electrode	1.5	0.7	0.05	[a]
Current collector of negative electrode	8.96	0.385	3.98	27
Electrode material of negative electrode	2.5	0.7	0.05	[a]
Separator	1.2	0.7	0.01	[a]
Pouch	1.15	1.9	0.16×10^{-2}	

[a]Measured at GM R&D Center.

where k is the rate constant of chemical reactions (s^{-1}; for the first order reaction), A is the pre-exponential factor (s^{-1}; for the first order reaction), E_a is the activation energy (J mol^{-1}), and R is the gas constant (J mol^{-1} K^{-1}). The functional relationship of U with T_{abs} suggested in Eq. 11 was deduced from the Nernst equation which gives the relationship between the equilibrium potential of the battery cell and the absolute temperature[22]

$$E = E^0 - \frac{RT_{abs}}{zF} \ln Q \quad [13]$$

where E is the cell potential (V), E^0 is the standard cell potential (V), z is the number of moles of electrons transferred in the cell reaction, and Q is the reaction quotient. The values of C_1 and C_2 used in this work were 1800 and -9.5×10^{-4}, respectively.

By solving the equations listed above, the distribution of the current density, J, on the electrodes can be obtained as a function of the position on the electrode and time. Therefore, the *DOD* varies with the position on the electrode and time elapsed during discharge. The distribution of *DOD* on the electrode can be calculated from the distribution of J as follows

$$DOD = \frac{\int_0^t J dt}{Q_T} \quad [14]$$

where t is the charge time (s), and Q_T is the theoretical capacity per unit area (Ah m^{-2}) of the electrodes.

The thermal modeling procedure employed to calculate the temperature distribution on the electrodes is similar to that used by Kim et al.[19,20] Since the thickness of the battery cell is much shorter than its other dimensions, the temperature variation along the z direction in Fig. 1 can be neglected. Based on the differential energy conservation for a battery, the transient two-dimensional equation of heat conduction can be written as follows

$$\rho C_p \frac{\partial T}{\partial t} = \frac{\partial}{\partial x}\left(k_x \frac{\partial T}{\partial x}\right) + \frac{\partial}{\partial x}\left(k_y \frac{\partial T}{\partial y}\right) + q - q_{conv} \quad [15]$$

where ρ is the density (kg m^{-3}), C_p is the volume averaged specific heat capacity at constant pressure (J kg^{-1} $°C^{-1}$), T is the temperature (°C), k_x and k_y are the effective thermal conductivities along the x and y directions (refer Fig. 1 for the x and y directions) (W m^{-1} $°C^{-1}$), respectively, q is the heat generation rate per unit volume (W m^{-3}), and q_{conv} is the heat dissipation rate (W m^{-3}) through the surfaces of the battery by convection. The effective thermal conductivities of the various compartments of the cell can be estimated based on the equivalent networks of the parallel and series thermal resistances of the cell components.[7,18]

The heat generation rate, q, is given as follows

$$q = aJ\left[E_{oc} - E - T\frac{dE_{oc}}{dT}\right] + a_p r_p i_p^2 + a_n r_n i_n^2 \quad [16]$$

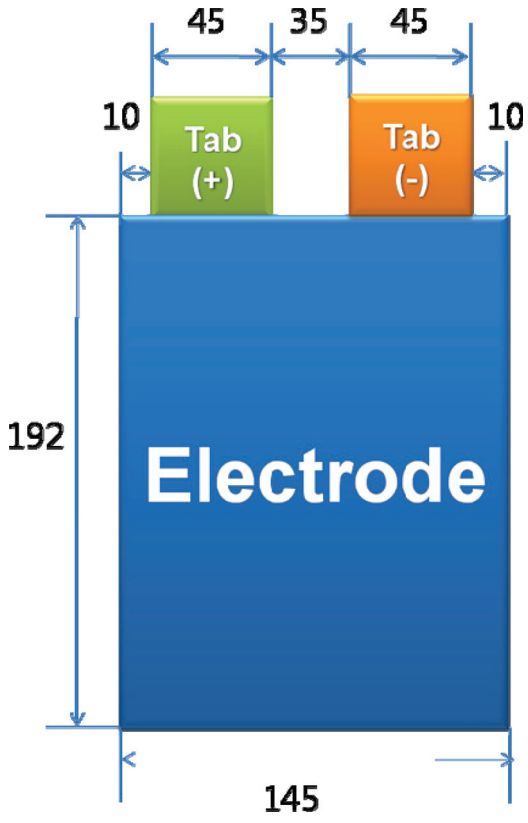

Figure 2. (Color online) The dimensions of the electrodes and the positions of the tabs of a 14.6 Ah LIB from LG Chem.

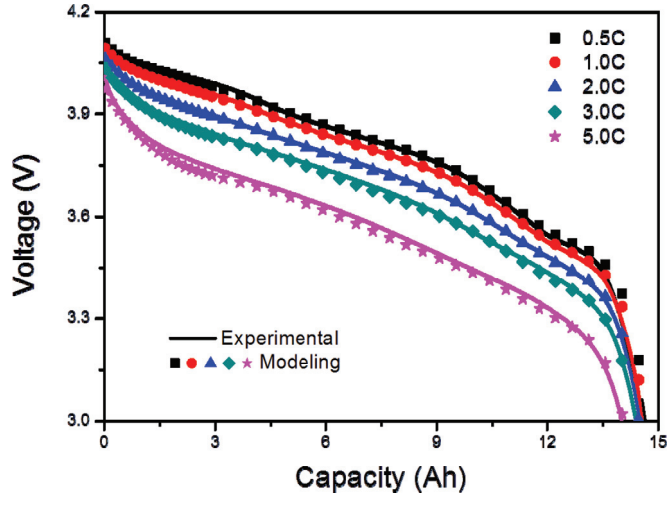

Figure 3. (Color online) Comparison of the experimental and modeling discharge curves at discharge rates ranging from 0.5 to 5 C for the LIB at an environmental temperature of 25°C.

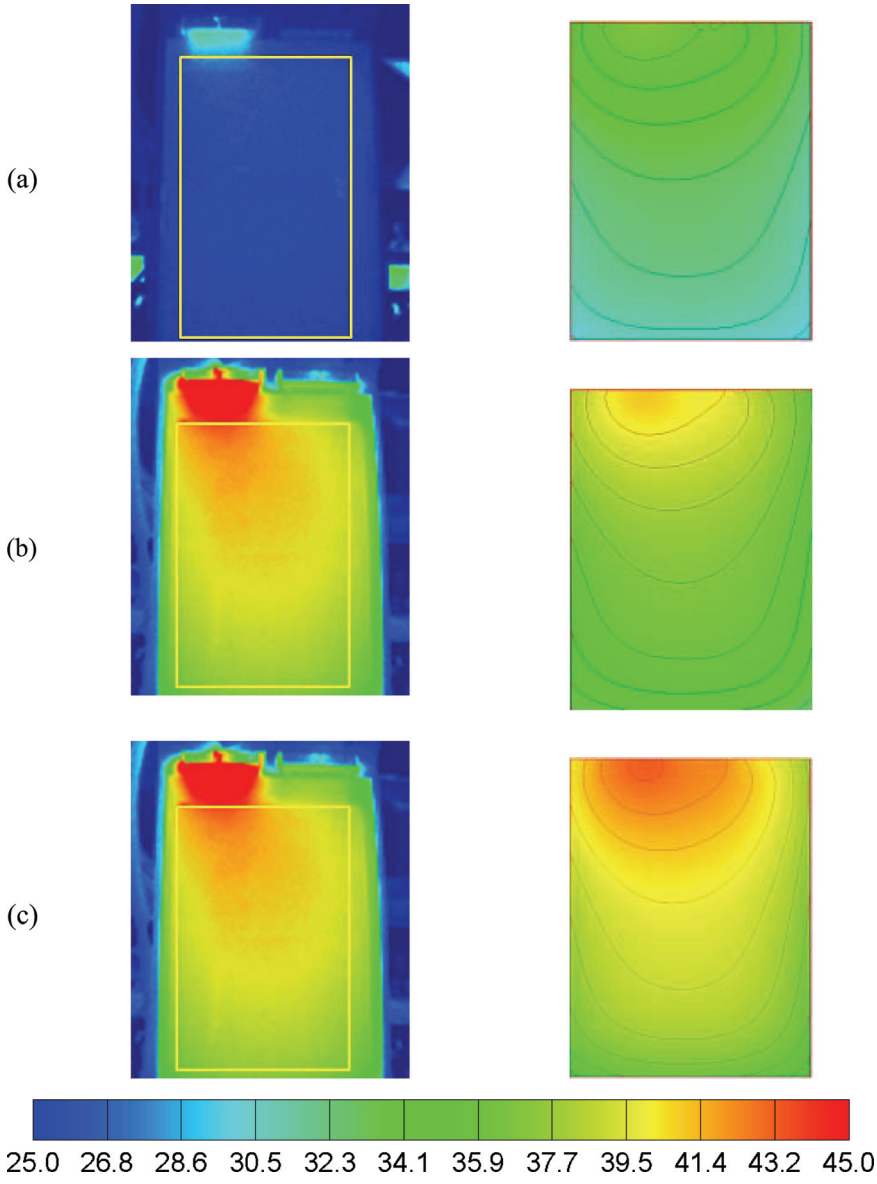

Figure 4. (Color online) Temperature distributions based on the experimental IR image and the modeling for the LIB at the discharge times of (a) 1, (b) 6, and (c) 11 min during discharge at a rate of 5 C and the environmental temperature of 25°C.

where a is the specific area of the battery (m^{-1}), J is the current density (A m^{-2}) calculated by Eq. 7, E_{oc} is the open-circuit potential of the cell (V), E is the cell voltage (V), a_p and a_n are the specific area of the positive and negative electrodes (m^{-1}), respectively, and i_p and i_n are the magnitudes of the vectors $\vec{i}_p$ and $\vec{i}_n$ obtained by Eqs. 3 and 4 (A m^{-1}), respectively. The detailed definition of each term on the right-hand side of Eq. 16 is described in Refs. 16, 19, and 26. The heat dissipation rate, q_{conv}, is derived as follows

$$q_{conv} = \frac{2h}{d}(T - T_{air}) \quad [17]$$

where h is the convective heat transfer coefficient on the surfaces of the battery (W m^{-2} $°C^{-1}$), d is the thickness of the battery in the direction perpendicular to the parallel electrodes (m), and T_{air} is the ambient temperature (°C). This term is rendered by approximating a three-dimensional object into a two-dimensional one, as shown in Eq. 15. The convective boundary condition applied to the boundaries of the electrode is the one reported by Kim et al.[19] Table II lists the parameters used for the thermal modeling.

Results and Discussion

The solutions to the governing Eqs. 5, 6 and 15 subject to the associated boundary conditions were obtained using the finite element method. In order to test the validity of the model, discharge experiments were carried out at room temperature of 25°C using a 14.6 Ah battery fabricated by LG Chem., of which the dimensions of the electrodes and the positions of the tabs are shown in Fig. 2. Figure 3 shows a comparison between the discharge curves calculated from the model and the experimental data for discharge rates ranging from 0.5 to 5 C at 25°C. At the various discharge rates ranging from 0.5 to 5 C, the experimental discharge curves are in good agreement with the modeling results based on the finite element method.

After obtaining the distributions of the potential and current density on the electrodes during discharge, the temperature distributions of the battery can be calculated as a function of time at various discharge rates using Eq. 15. As a demonstration, Figs. 4a–4c show the temperature distributions based on the experimental IR image and the modeling for the 14.6 Ah LIB at an environmental temperature

of 25°C at discharge times of 1, 6 and 11 min during discharge with a rate of 5 C. In the IR images, the region within the yellow lines of the rectangle corresponds to the computational domain used for the modeling. Therefore, the maximum temperature within the computational domain should be differentiated from that of the current collecting tab protruding beyond the electrode region of the battery cell. The overall temperature distributions obtained from the experiment and model in Figs. 4a–4c are in good agreement with each other. The temperature near the current collecting tab of the positive electrode is higher than that of the negative electrode. This was attributed to the electrical conductivity of the active material of the positive electrode being much lower than that of the negative electrode, even though the current flows near the tabs of both the positive and negative electrodes are similarly high. Figures 5a and 5b show the maximum and minimum temperatures obtained from the experimental measurements and those predicted by the model, respectively. The maximum and minimum temperatures obtained from the experiment and modeling were in good agreement with each other over the whole range of DODs at the various discharge rates. However, the discrepancy between the minimum temperatures obtained from the experiment and modeling was higher than that between the corresponding maximum ones. As can be seen in Fig. 4, the minimum temperatures were observed at the corners of the electrodes, where the effect of the two-dimensional approximation of the three-dimensional battery on the accuracy of the thermal modeling is maximal. Therefore, the two-dimensional model in this work was unable to

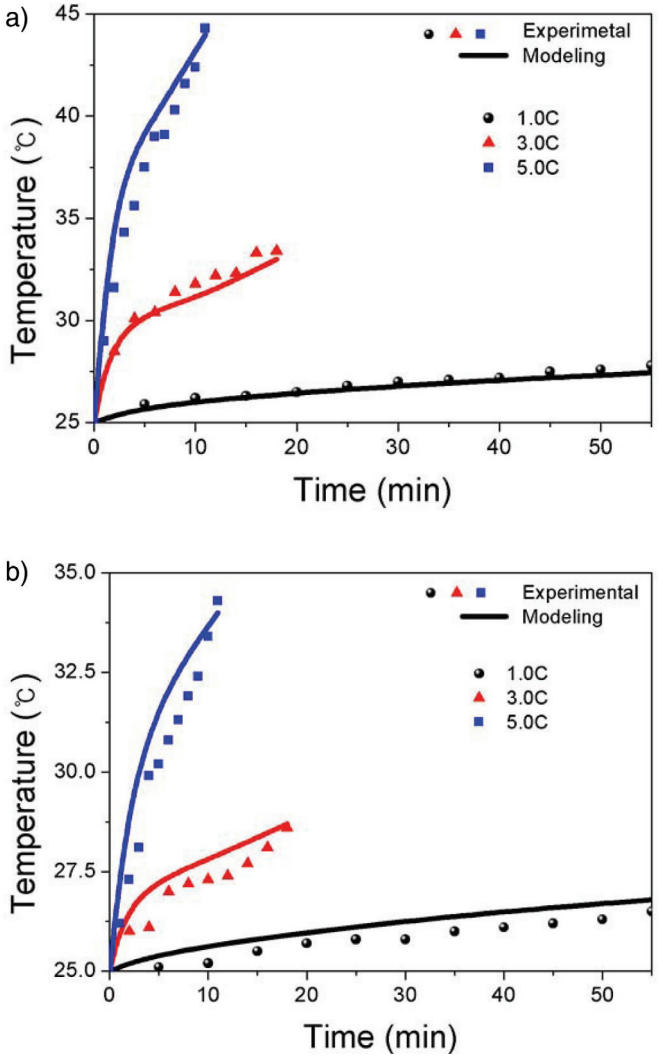

Figure 5. (Color online) Comparison of the (a) maximum temperatures and (b) minimum temperatures obtained from the experiment and model for the LIB during discharge at discharge rates of 1, 3 and 5 C and an environmental temperature of 25°C.

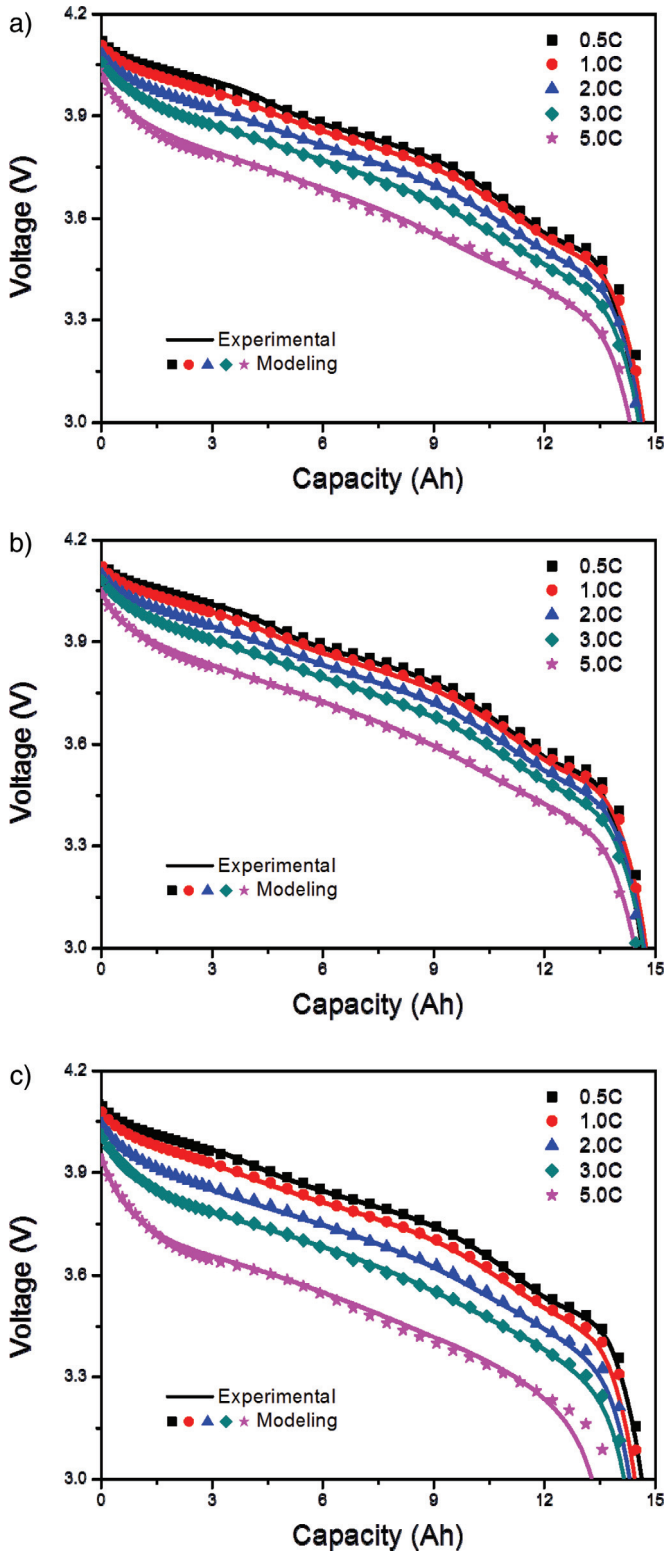

Figure 6. (Color online) Comparison of the experimental and modeling discharge curves at discharge rates ranging from 0.5 to 5 C for the LIB at environmental temperatures of (a) 35, (b) 45, and (c) 15°C.

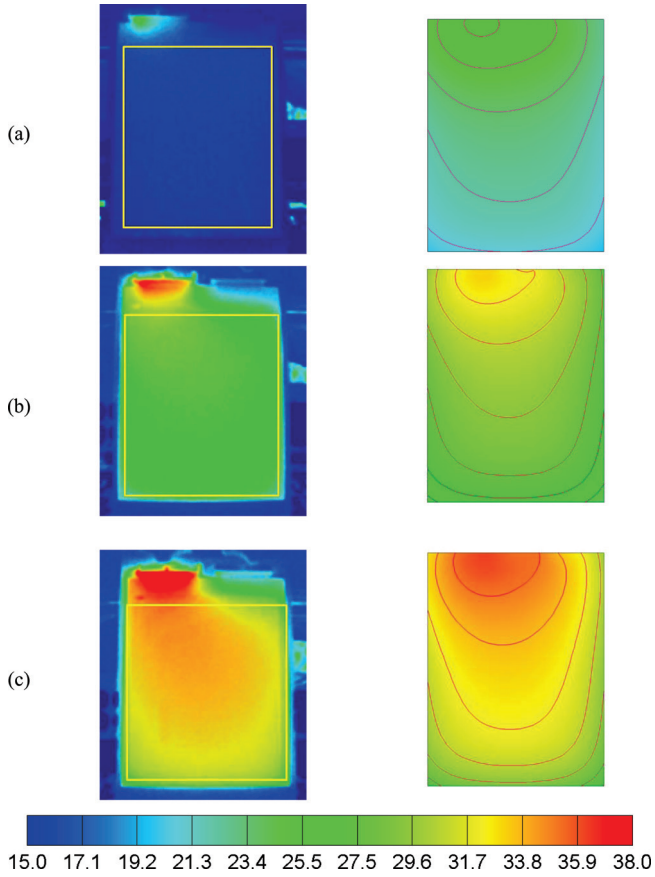

Figure 7. (Color online) Temperature distributions based on the experimental IR image and the modeling for the LIB at discharge times of (a) 1, (b) 6, and (c) 11 min during discharge at a rate of 5 C and environmental temperature of 15°C.

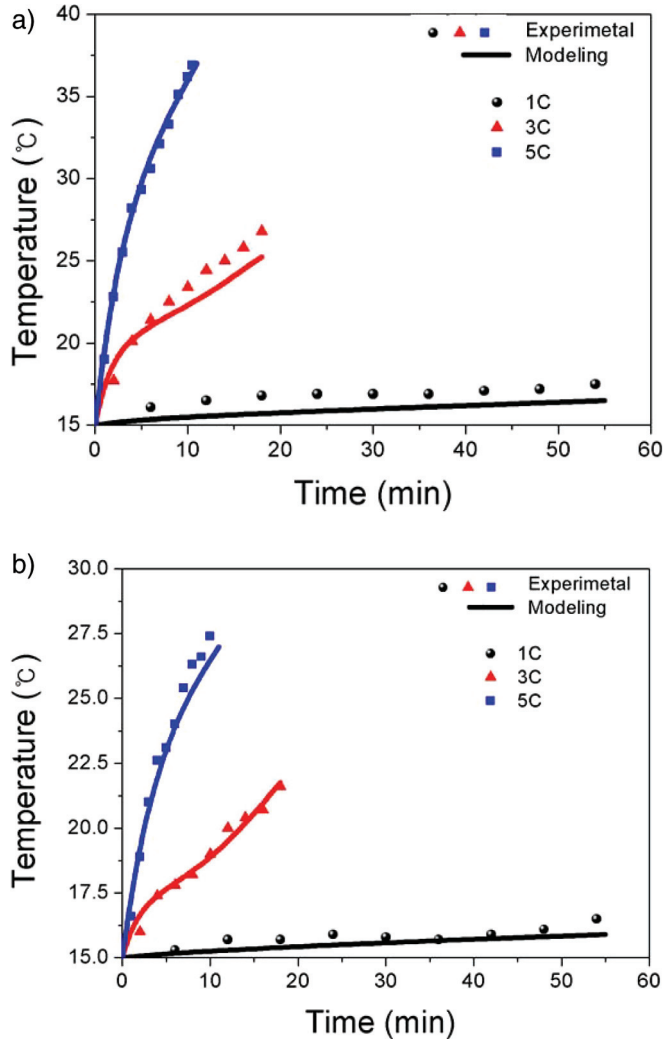

Figure 8. (Color online) Comparison of the (a) maximum temperatures and (b) minimum temperatures obtained from the experiment and model for the LIB during discharge at discharge rates of 1, 3 and 5 C and an environmental temperature of 15°C.

pick up the physics of the system accurately as regards the minimum temperatures. The ability of the model to describe the minimum temperatures might be improved, if it is extended to three-dimensional, which is beyond the scope of this work.

Figures 6a and 6b show the comparisons between the calculated discharge curves obtained from the model and the experimental data for discharge rates ranging from 0.5 to 5 C at the environmental temperatures of 35 and 45°C, respectively. The experimental discharge curves agree well with those obtained from the modeling at environmental temperatures of 35 and 45°C. This means that the modeling methodology used for the potential and current density distributions on the electrodes at an environmental temperature of 25°C can be safely extended to the environmental temperatures up to 45°C by using Eqs. 10 and 11. Figure 6c shows the comparisons between the discharge curves obtained from the model and those obtained from the experiment at an environmental temperature of 15°C. The experimental discharge curves agree well with those obtained from modeling at an environmental temperature of 15°C, although the discharge curve obtained from the modeling deviates from the experimental one near the end of discharge with a discharge rate of 5 C. This means that the potential and current density distributions on the electrodes at an environmental temperature of 25°C can be extended to an environmental temperature of 15°C by using Eqs. 10 and 11, with the possible exception of discharge rates higher than 5 C, for which some discrepancy was observed between the discharge curves obtained from the model and experiment near the final stage of discharge.

Figures 7a–7c show the temperature distributions based on the experimental IR images and modeling at discharge times of 1, 6 and 11 min during discharge at a rate of 5 C under the environmental temperature of 15°C. The overall temperature distributions obtained from the experiment and model in Figs. 7a–7c are in good agreement with each other as in the case of those at an environmental temperature of 25°C shown in Figs. 4a–4c. Figures 8a and 8b show the maximum and minimum temperatures at an environmental temperature of 15°C obtained from the experimental measurements and those predicted by the model, respectively. The maximum and minimum temperatures obtained from the experiment and modeling are in good agreement with each other over the whole range of DODs at the various discharge rates. In Figs. 9a–9c, the temperature distributions based on the experimental IR image and the modeling at the discharge times of 1, 6 and 11 min during discharge at a rate of 5 C and environmental temperature of 45°C were compared with those obtained from the model. The maximum and minimum temperatures at an environmental temperature of 45°C obtained from the experimental measurements and those predicted by the model are shown in Figs. 10a and 10b, respectively. The overall temperature distributions and maximum and minimum temperatures obtained from the experiment are also in good agreement with those obtained from the modeling for an environmental temperature of 45°C. We also confirmed the good agreement between the thermal behaviors during

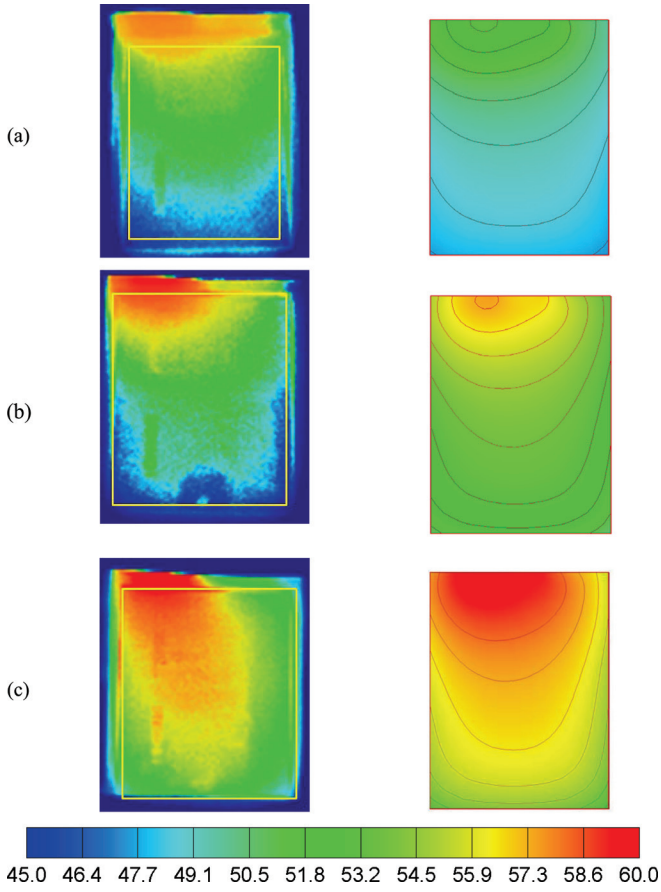

Figure 9. (Color online) Temperature distributions based on the experimental IR image and the modeling for the LIB at discharge times of (a) 1, (b) 6, and (c) 11 min during discharge at a rate of 5 C and an environmental temperature of 45°C.

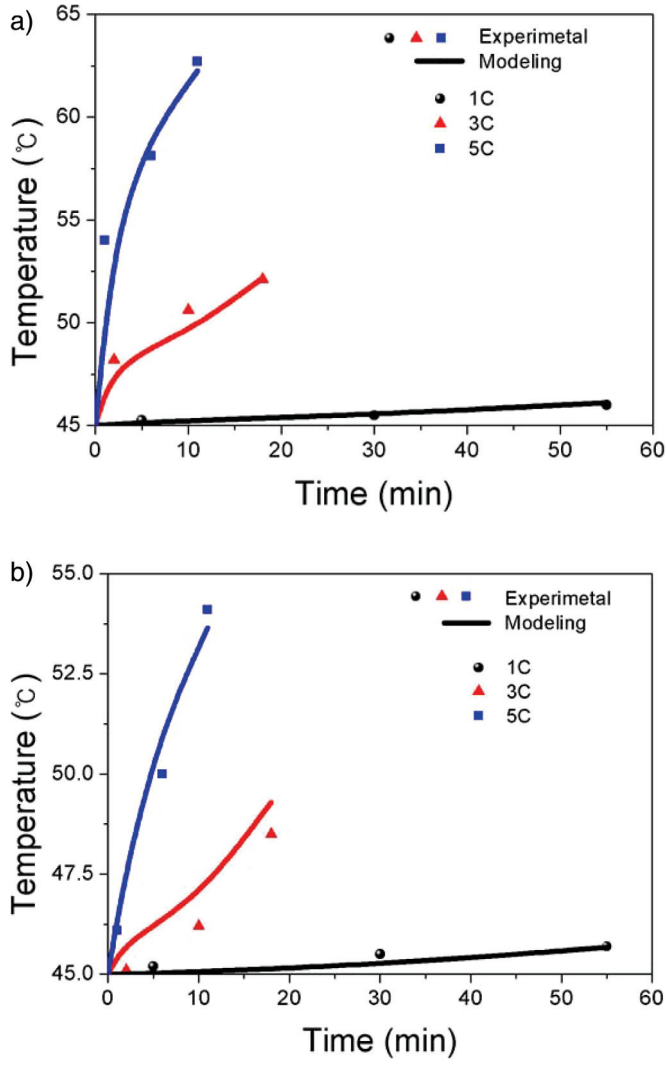

Figure 10. (Color online) Comparison of the (a) maximum temperatures and (b) minimum temperatures obtained from the experiment and model for the LIB during discharge at discharge rates of 1, 3 and 5 C and an environmental temperature of 45°C.

discharge observed from the experiment and those from the modeling at an environmental temperature of 35°C, but we did not include these results since they appeared to be redundant.

Conclusions

A mathematical procedure was developed to study the dependence of the discharge behaviors of an LIB on the environmental temperature. The two-dimensional potential and current density distribution on the electrodes of the LIB were predicted as a function of the discharge time by using the finite element method. By comparing the experimental discharge curves with the modeling results at various discharge rates and the environmental temperatures of 15, 25, 35, and 45°C, the modeling of the dependence of the potential and current density distributions of the LIB on the environmental temperature was validated. Then, based on the results of the modeling of the potential and current density distributions, the heat generation rate as a function of the discharge time and position on the electrodes was calculated to predict the thermal behavior of the LIB. The two-dimensional temperature distributions obtained from the experiment and modeling were in good agreement with each other during the whole process of discharge at various discharge rates and environmental temperatures ranging from 15 to 45°C. The modeling methodology presented in this study may contribute to the development of a battery management algorithm which allows the performance of LIB as a function of the environmental temperature to be more accurately predicted.

Acknowledgments

This study was supported by General Motors Corporation. One of the authors (C. B. Shin) acknowledges the partial financial support provided by the National Research Foundation of Korea (NRF 2009-0064626 and NRF 2010-0025353) and the Ministry of Commerce, Industry and Energy of Republic of Korea (2007-E-1D25-P-02-0-00) for this work.

Ajou University assisted in meeting the publication costs of this article.

References

1. G. Cedar, M. Doyle, and P. Arora, Y. Fuentes, *MRS Bull.*, **27**, 619 (2002).
2. J. Newman, K. E. Thomas, H. Hafezi, and D. R. Wheeler, *J. Power Sources*, **119–121**, 838 (2003).
3. H. J. Bergveld, W. S. Kruijt, and P. H. L. Notten, *Battery Management Systems: Design by Modelling*, 1st ed., Kluwer Academic Publishers, Dordrecht (2002).
4. M. Doyle, T. F. Fuller, and J. Newman, *J. Electrochem. Soc.*, **140**, 1526 (1993).
5. M. Doyle and J. Newman, *J. Power Sources*, **54**, 46 (1995).
6. Y. Chen and J. W. Evans, *J. Electrochem. Soc.*, **140**, 1833 (1993).
7. Y. Chen and J. W. Evans, *J. Electrochem. Soc.*, **141**, 2947 (1994).
8. Y. Chen and J. W. Evans, *J. Electrochem. Soc.*, **143**, 2708 (1996).
9. C. R. Pals and J. Newman, *J. Electrochem. Soc.*, **142**, 3274 (1995).
10. C. R. Pals and J. Newman, *J. Electrochem. Soc.*, **142**, 3282 (1995).

11. M. W. Verbrugge, *AIChE J.*, **41**, 1550 (1995).
12. G. G. Botte, B. A. Johnson, and R. E. White, *J. Electrochem. Soc.*, **146**, 914 (1999).
13. S. Al-Hallaj, H. Maleki, J. S. Hong, and J. R. Selman, *J. Power Sources*, **83**, 1 (1999).
14. L. Song and J. W. Evans, *J. Electrochem. Soc.*, **147**, 2086 (2000).
15. W. B. Gu, and C. Y. Wang, in *Lithium Batteries*, S. Surampudi, R. A. Marsh, Z. Ogumi, and J. Prakashi, Editors, PV 99-25, p. 748, The Electrochemical Society Proceeding Series, Pennington, NJ (2000).
16. V. Srinivasan and C. Y. Wang, *J. Electrochem. Soc.*, **150**, A98 (2003).
17. P. M. Gomadam, R. E. White, and J. W. Weidner, *J. Electrochem. Soc.*, **150**, A1339 (2003).
18. S. C. Chen, C. C. Wan, and Y. Y. Wang, *J. Power Sources*, **140**, 111 (2005).
19. U. S. Kim, C. B. Shin, and C.-S. Kim, *J. Power Sources*, **180**, 909 (2008).
20. U. S. Kim, C. B. Shin, and C.-S. Kim, *J. Power Sources*, **189**, 841 (2009).
21. K. H. Kwon, C. B. Shin, T. H. Kang, and C.-S. Kim, *J. Power Sources*, **163**, 151 (2006).
22. A. J. Bard and L. R. Falkner, *Electrochemical Methods: Fundamentals and Applications*, 2nd ed., John Wiley and Sons, Inc., New York (2001).
23. W. Tiedemann and J. Newman, in *Battery Design and Optimization*, S. Gross, Editor, PV 79-1, p. 39, The Electrochemical Society Proceeding Series, Pennington, NJ (1979).
24. J. Newman and W. Tiedemann, *J. Electrochem. Soc.*, **140**, 1961 (1993).
25. H. Gu, *J. Electrochem. Soc.*, **130**, 1459 (1983).
26. C. Y. Wang and V. Srinivasan, *J. Power Sources*, **110**, 364 (2000).
27. S. C. Chen, C.C. Wan and Y. Y. Wang, *J. Power Sources*, **140**, 111 (2005).